Impact of Holmium and Nickel Substitution on Y-Type Hexagonal Ferrites Synthesized via Sol-gel Method

Alina Manzoor[1*], Aamir Shahzad[1], Muhammad Imran Arshad[1], Amir Muhammad Afzal[2], Tauqir Shinwari[3*], Muhammad Yaqoob Khan[4]

[1] Department of Physics, Government College University Faisalabad, Faisalabad-38000, Pakistan
[2] Department of Physics, Riphah International University, 13-km Raiwind Road, Lahore-54000, Pakistan
[3] Institut für Experimentalphysik, Freie Universität Berlin, 14195 Berlin, Germany
[4] Department of Physics, Kohat University of Science and Technology, Kohat-26000, Khyber Pakhtunkhwa, Pakistan

ARTICLE INFO

ABSTRACT

Sol-gel auto combustion route is employed to fabricate Y-type hexagonal ferrites $Ba_{2-x}Ho_xSr_{2-y}Ni_yFe_{12}O_{22}$(x = 0, 0.02, 0.04, 0.06, 0.08, 0.1 & y = 0, 0.1, 0.2, 0.3, 0.4, 0.5). All prepared samples are examined through XRD, SEM, and dielectric characterization.The prepared samples were then sintered at 950 °C for 6 hours. TGA analysis was carried out to find the estimated sintering temperature for the phase development. The XRD experiment was performed to determine the effect of substitution on structural parameters. XRD crystallite size was observed in the range of 5.5 – 19.79 nm. Lattice constant (a) was found in the range 6.08 – 6.17 Å, and that of c was found in the range 44.08 – 44.73 Å. The averagegrain size value wasnoted to be around ~ 2µm as calculated through SEM.Through Raman spectroscopy, six active modes ($3E_{1g}$, $2A_{1g}$, and E_{2g}) correspond to different vibrational modes of the prepared samples. LCR technique showed that the dielectric constant and the dissipation factor were decreased with increased frequency. A decrease in dielectric losses suggests these materials are for high-frequency applications.

*Corresponding Authors' Email: alinamanzoor@hotmail.com, t.tauqir@fu-berlin.de

1.   Introduction

In the competition of new creations, new technological materials have acquired much more courtesy due to their direct convenience, particularly in material science. Hexagonal ferrites have attracted much attention since their discovery by Philips in the 1950s(Irfan, Elahi, & Shakoor, 2016).Due to their extraordinary magnetic properties, ferrites are the most widely utilized materials. Due to their high stability, electrical resistance, and ferromagnetism, these materials are frequently used in permanent magnets, magnetic recorders, memory chips, and microwave devices. The structure of different ferrites differs from each other due to their structure, like spinel ferrites, ortho-ferrites, garnets, and hexagonal ferrites(Chen, Wang, Liu, Jin, & Wu, 2022; C.-h. Wang et al., 2022). Due to their low cost, ease of manufacture, and exceptional electrical, dielectric, and magnetic properties, hexa-ferrites have attracted much attention in the technological areas in recent decades(Lan, Zhao, Gao, Kou, & Wu, 2021; Narang & Pubby, 2021). Manufacturing factors, such as composition, doping type and amount, sintering temperature and time, etc., significantly impact the materials' performance. Due to their use in multilayer chip inductors, microwave devices, and magnetic recording, they are currently regarded as materials in demand (Houbi et al., 2021). Based on their crystal structure and chemical makeup, these ferrites can be divided into six main categories: M, W, Y, X, Z, and U-type hexa-ferrites. These hexa-ferrites differ from each other.

The different super-positioned configurations of the R, S, and T building components in these hexa- ferrites distinguish them (Ali et al., 2015). Y-type hexa-ferrites are a composite of hexagonal barium M-type ferrite and cubic spinel ferrites, which are among these hexagonal ferrites.Although they have a complicatedstructure, they have a hexagonal structure parallel to the c-axis(Ali et al., 2014). As a result, Y-type ferrites have a self-biased magnetic field that is uniaxial anisotropic and normal to the c-axis. As a result, Y-type ferrites have a self-biased uniaxial magnetic anisotropic field and an easy axis of magnetization that is normal to the c-axis.

Consequently, they have a preferred plane to align the saturation magnetization, which can be chosen as a plane of microwave devices(Batool et al., 2022).Hexa-ferrites are used in a high-density magnetic recording medium, which calls for materials that can be precisely controlled in terms of homogeneity, shape, and magnetic characteristics. Finding the most significant creation conditions to obtain tiny particles for use in high-density magnetic recording media is essential. The sol-gel, the chemical co-precipitation, sol-gel, microemulsion, hydrothermal synthesis, and opposite micelle(Irfan et al., 2016; Jacobo, Domingo-Pascual, Rodriguez-Clemente, & Blesa; Kumazawa, Maeda, & Sada, 1995; Pillai, Kumar, & Shah, 1992; Zhong & Ding, 1997). In the current study, doping with a relatively small amount of Y_2O_3 significantly alters the morphological, dielectric, and magnetic characteristics of Y-type hexa-ferrites.As mentioned earlier, the variation of the properties is appropriate for their applications in various electrical devices working for industrial and military applications.Hexagonal ferrites have varied applications in multiple devices, such as high-density magnetic recording systems, microwave devices, frequency telecommunication devices, biomedical applications (like cellular imaging, hyperthermia, target drug delivery, etc.), and cores of inductors.Since the sol-gel auto-combustion method is straightforward in composition and shape, it has been utilized to create homogeneous nano-crystallites of hexagonal ferrites(Irfan et al., 2016).

Hexagonal ferrites give high permeability in RF (radio frequency). This feature founds numerous applications in devices like micro-inductors and antennas(Liu et al., 2018). Hard ferrites or hexagonal ferrites have found multiple applications in telecommunication technology. They can be made devices applicable to high-range electromagnetic wave devices, which is very important for distortion-free telecommunication (Majeed et al., 2016). Ferrites with different cationic substitutions at various sites are useful in industrial and technological applications. Due to unique properties of hard ferrites such as less electro-conductivity than metallic ferrites, high permeability, high Curie temperature (T_c), high value of M_s, high value of coercivity (H_c), and high remanence after the magnetic field and low eddy current lose made them very effective in different industrial and technological applications (Din et al., 2014).

At room temperature, nickel is a very oxidation-resistant and ferromagnetic metal. Because rare earth metals significantly affect the system's magnetic anisotropy, spinel ferrite is promising. Holmium and nickel-substituted Y-type hexagonal ferrites are Y-type hexagonal ferrites in which part of the yttrium (Y) ions in the crystal structure have been changed to holmium (Ho) and nickel (Ni) ions. Hexa-ferrites have magnetic properties widely used in various applications, including magnetic storage devices, microwave devices, and permanent magnets(Yang & Wang, 2017). They are also referred to as hexagonal ferrites or ferrite magnets. Holmium and nickel ions can be utilized to swap out yttrium ions, altering the properties of Y-type hexagonal ferrites. Adding extra magnetic moments to the crystal lattice caused by the substitution of holmium can change the material's magnetic characteristics(Aslibeiki, 2014). Nickel replacement may also impact the ferrite's magnetic and structural properties.

2.   Experimental Procedure

To synthesize $Ba_{2-x}Ho_xSr_{2-y}Ni_yFe_{12}O_{22}$hexagonal ferrites,the following extremely pure materials such as $Ni(NO_3)_2.6H_2O$, $Fe(NO_3)_3.9H_2O$, $Ho(NO_3)_3.5H_2O$, $Ba(NO_3)_2$ and $Sr(NO_3)_2$ were used. For the preparation of the solution, deionized distilled water was used. Holmium and nickel substituted Y-type hexagonal ferrites with a nominal composition of $Ba_{2-x}Ho_xSr_{2-y}Ni_yFe_{12}O_{22}$(x = 0, 0.02, 0.04, 0.06, 0.08, 0.1 and y = 0, 0.1, 0.2, 0.3, 0.4, 0.5) were prepared by Sol-gel method. The prepared solutions were then stirred using a magnetic stirrer. After the stirring of all these solutions, all the solutions were then combined into a

single beaker while keeping the stirring ON. The stirring was kept ON until the formation of a homogeneous solution. The pH of the solution was kept at seven by adding NH_3 solution dropwise. After attaining the desired pH, the heat was turned ON while keeping the stirring ON. After 4 hours of heat treatment, the solution was converted into the xerogel; by further heating, the xerogel was then converted into the ash. The ash was then ground to make the fine powder. After that, the fine powders were sintered at 950 ℃ for 6 hours. After sintering, the samples were ground well in the mortar and pestle to make the fine powder. In the end, the prepared samples were poured into the append drops in powder form, and some of the material was used to make pellets using a hydraulic press to study dielectric and I-V characterizations.

To check the required phase of hexagonal ferrites of the crystal structure of the prepared sample were identified by XRD. SEM calculated the grain size of hexagonal ferrites. For the energy bandgap of all samples using UV- visible spectroscopy. To check the dielectric response of materials in the 1 KHz-1MHz frequency range was observed with an impedance analyzer.

3.   Results and Discussion
3.1.   TGA Analysis

Thermo-Gravimetric Analysis (TGA) is a method for determining how much a sample weighs changes to temperature or time. It is frequently used to examine the materials' moisture content, thermal stability, and decomposition behavior. Figure 1 shows the TGA curve of fabricated Y-type hexagonal ferrites with chemical composition $Ba_2Sr_2Fe_{12}O_{22}$. This approach helps one to track the sample's weight loss with the increase in temperature. About 3% weight loss was obtained at 67 ℃, indicating the water's dryness, which was physically absorbed by the sample. However, almost 3% weight loss was observed at 606 ℃, indicating organic compounds' oxidation decomposition. However, after 765℃, no noticeable change in the weight loss was observed, which ensures the beginning of hexagonal ferrite phase formation(Ahmad et al., 2015).

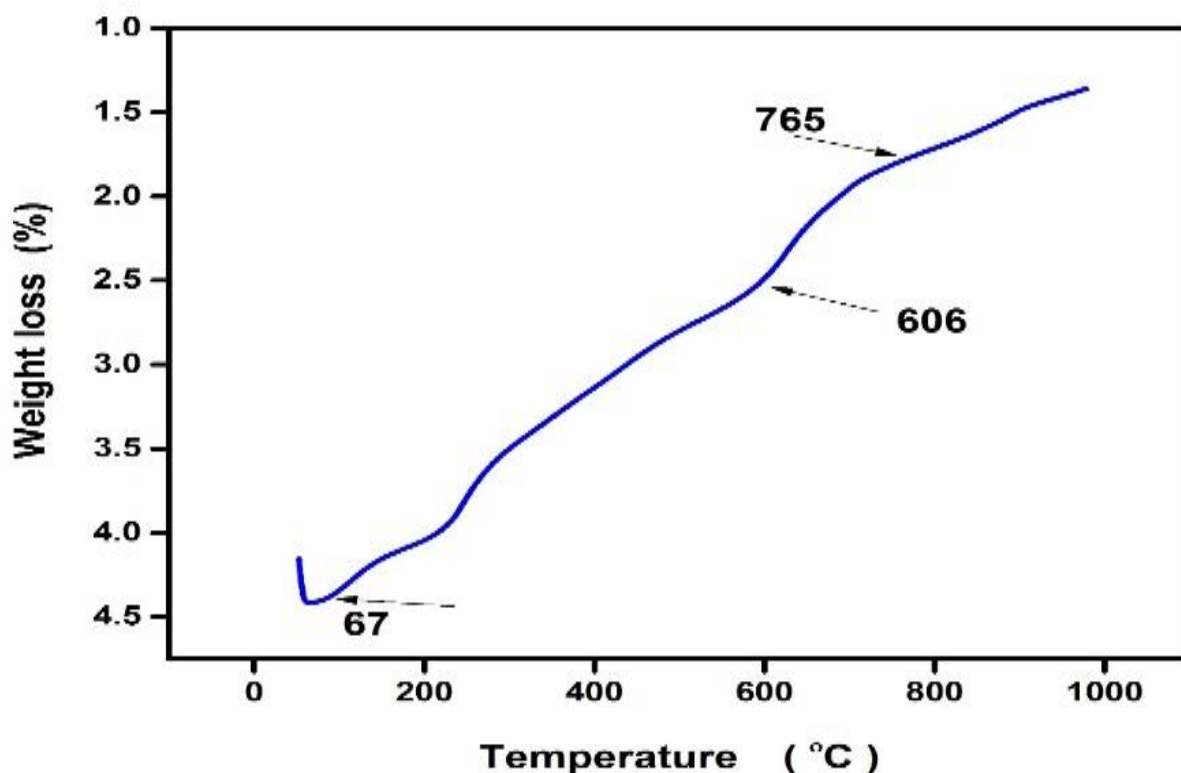**Figure 1: Temperature vs weight loss curve of$Ba_2Sr_2Fe_{12}O_{22}$**

3.2. XRD Analysis

Figure 2 shows the XRD patterns of the holmium and nickel-substituted Y-type hexagonal ferrites withthe composition of $(Ba_{2-x}Ho_xSr_{2-y}Ni_yFe_{12}O_{22})$with($x = 0$-$0.1$ and $y = 0$-0.5) were prepared by Sol-gel method.The XRD patterns confirm the hexagonal structure of holmium and nickel-doped Y-type ferrites. Phase examines investigations were made by comparing the obtained XRD patterns with JCPDS data file No. 00-051-1879. All the peaks in XRD patterns were compared with the standard JCPDS data.The diffraction peaks seen from these XRD patterns correspond to the different planes described as (110), (0114), (021), (2011), (0219),and (2113). It is determined from these miller indices that the fabricated material has a hexagonal structure(Elahi, Ahmad, Ali, & Rana, 2013). The main peak is observed at $\theta = 29.286°$, and the crystallite size for this peak is calculated to be 26.8 nm. At the same time, the crystallite size of other peaks (0114), (021), (2011), (0219), and (2113)are also calculated and found to be 28.52 nm, 14.22 nm, 16.56 nm, and 12.87 nm, respectively. The average crystallite size is found to be 19.80 nm. From Figure 2, it is clear that when the Ho-Ni concentration rises, the intensity of some peaks decreases (Rezlescu, Istrate, Rezlescu, & Luca, 1974). It is noted that there is no peak splitting. Different parameters are calculatedusing XRD data, such as crystallite size, FWHM, lattice constants, etc. For all categories of hexagonal ferrites "c," axis is considered the major axis. Large variations in lattice constant "c" are more well-known than in "a"(J. Wang, Ponton, & Harris, 2006). The c/a ratio values also established the y-type hexagonal structure. The following Scherrer's formula calculates the crystallite size:

$$D = \frac{k\lambda}{\beta cos\theta}$$

(1)

Here, D represents the crystalline size in nm,K is Scherer constant, and its value is 0.94 for Y-type hexagonal structure,λ gives the X-rays wavelength,β represents the full-width half maxima value of different peaks, andθ provides the Bragg's angle.
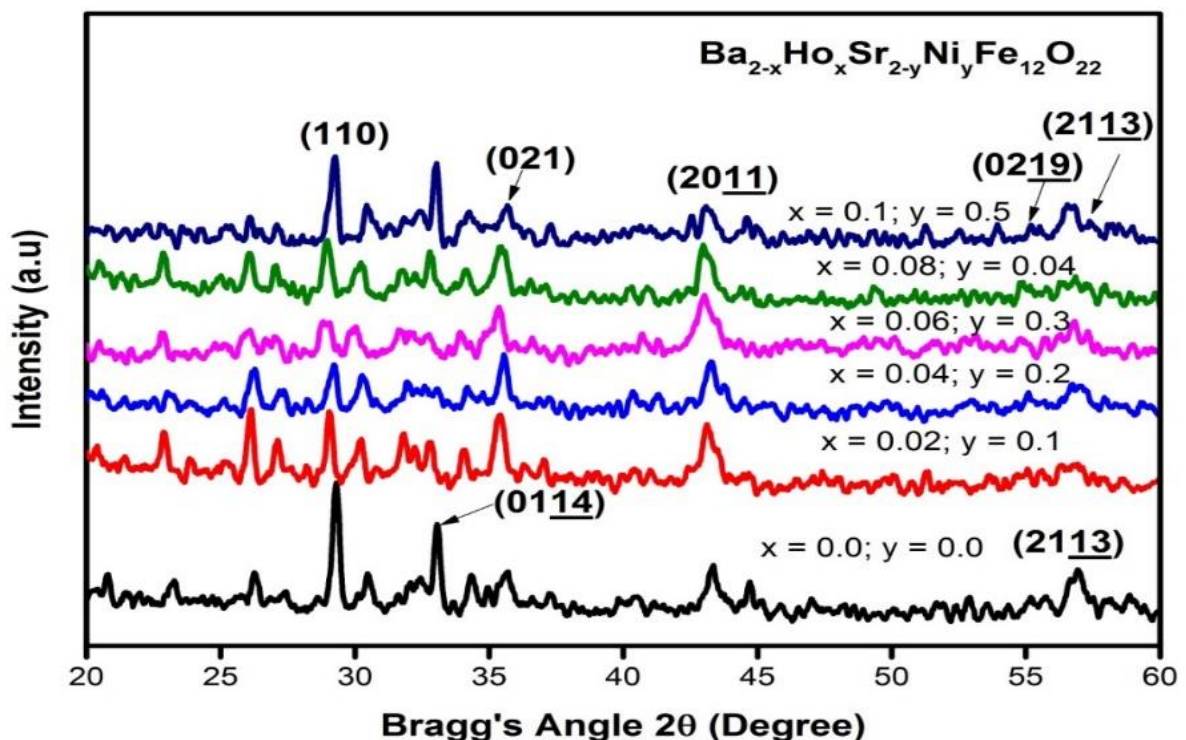
Figure 1: XRD patterns of $Ba_{2-x}Ho_xSr_{2-y}Ni_yFe_{12}O_{22}$ Ferrites

The calculated crystallite size ranges from 5.67 to 52.04nm.As Ho-Ni concentrations increased, the performance decreased, as shown by the size of the crystallites. Many investigators have found declining behavior caused by doping rare earth cations.Ho ions segregation, which occurs close to the grain borders and inhibits the movement of grain boundaries, is the cause of this reduction(Lassoued & Li, 2020; Pant, Arora, Kaur, Kumar, & Kumar, 2010).Lattice constants (a, c) are calculated using the formula(Ahmad et al., 2013).

$$\text{Sin}^2\theta = \frac{\lambda^2}{3a^2}(h^2 + hk + k^2) + \left(\frac{\lambda^2}{4c^2}\right)l^2 \tag{2}$$

Cell volume is found using the formula:

$$V = a^2 c \sin 120° \tag{3}$$

The d-spacing is found using the following formula:

$$d_{hkl} = \frac{\lambda}{2 \sin \theta} \tag{4}$$

The X-ray density is foundusing the formula:

$$d_x = \frac{ZM}{N_A V} \tag{5}$$

The unit cell volume of the prepared samples indicates an increasing trend, which is in good agreement with increasing dopants concentrations in y-type hexa-ferrites. Since lattice constants affect unit cell volume, a similar pattern is seen in both instances. The crystallite sizeranges from 5.67nm to 52.04nm. The range of lattice constants a and c is found to be 6.08-6.17Å and 44.15-44.73 Å,respectively.The cell volume ranges from 1411.13-1467.96 Å^3(Table 1).

Table 1
XRD parameters of Ba$_{2-x}$Ho$_x$Sr$_{2-y}$Ni$_y$Fe$_{12}$O$_{22}$ Y-typehexagonal ferrites

| Concentration	Angle 2θ (Degree)	Miller indices (hkl)	FWHM (Radian)	Crystallite size D (nm)	Lattice constant a (Å)	Lattice constant c (Å)	c/a ratio	Unit cell volume V (Å^3)
x= 0, y=0	29.30	110	0.299	26.812	6.08	44.08	7.25	1411.13
x= 0.02, y=0.1	29.08	110	1.543	52.045	6.14	44.52	7.25	14.53.48
x= 0.04, y=0.2	29.18	110	1.274	6.299	6.09	44.15	7.25	1418.02
x= 0.06, y=0.3	28.69	110	1.418	5.667	6.17	44.73	7.25	1474.76
x= 0.08, y=0.4	28.97	110	1.274	6.299	6.16	44.67	7.25	1467.96
x= 0.1, y=0.5	29.18	110	1.413	5.679	6.09	44.15	7.25	1418.02

3.3. Dielectric Analysis

The dielectric properties of prepared materials are investigated to determine the effect of doping fluctuations in the dielectric parameters. Electrostatic energy stored per unit volume is used to define the dielectric constant. Figures 3 and 4 depict the variations in the dielectric constant (ϵ')and tangent loss(ϵ'')for all samples at room temperature under a frequency range of 4 Hz to 8 MHz.The dielectric constant calculates the electrostatic energy retained per unit volume per unit gradient. The relative speed of an electromagnetic signal moving through a substance is measured using its dielectric constant. The dielectric constant is calculated using:

$$\epsilon' = \frac{Cp}{Co}, \text{ where} C_o = \frac{A\epsilon o}{d.} \tag{6}$$

Where $\dot{\epsilon}$ is the dielectric constant, Cp is parallel capacitance, ϵ_o is the permittivity of free space, A is the area of the pellet, and d is the thickness of the pellet. Figure 3 shows that the dielectric constant (ϵ') decreasesas the applied frequency increases. At much higher frequencies, it becomes frequency independent, which is the expected behavior of hexa-ferrites. Based on Koop's polarization theory and the Maxwell-Wagner model, which claims that dielectric ions and conductivity have the same origin root, charge carrier behavior, and hopping predictions between Fe^{3+} and Fe^{2+}, this result is attributed to space charge polarization. The chemical composition, fabrication process, sintering conditions, particle size, cation distribution, and other factors all affect the dielectric characteristics of hexagonal ferrites. As a function of frequency at room temperature, the dielectric constant (ϵ') is shown in the figure.

Dielectric polarization can be produced in the externally applied electric field because of the dielectric constant of the materials. The dielectric constant value also estimates the

speed of EM (Electromagnetic) signals. The dependence of the dielectric constant of Ho-Ni substituted Y-type hexagonal ferrites having composition Ba2-xHoxSr2-yNiyFe12O22 on the frequency in the range of (4Hz-8GHz) can be shown in figure 3. The dielectric constant was found to be decreasing with an increase in the frequency. That can be due to the exchange of Fe2+ and Fe3+ ions. Dispersion in the dielectric constant can be found due to the dipole's relaxation. Due to the irregular distribution of oxygen ions at grain boundaries and grain during sintering, interfacial polarization can occur. The dielectric constant in the ferrites is caused by the reduction of the field by the polarization effect. The dielectric constant is also caused by the electric, dipole, and ionic polarization at higher frequencies. The dipole and ionic polarization are found to be dominating in the microwave (GHz), and radio (MHz) frequency ranges(Yasmin et al., 2020).
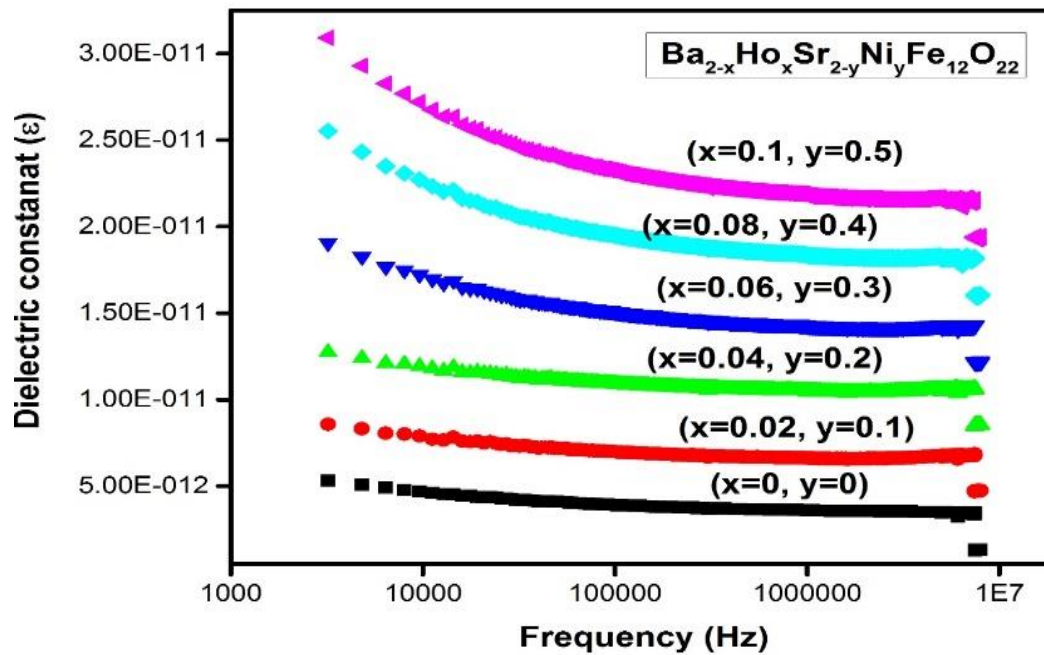
Figure 2: Frequency vs dielectric constant (ε') at room temperature

Dielectric loss illustrates the conduction of electrical energy from an external electric field within a dielectric substance. Dielectric losses (Ɛ") at room temperature as a function of frequency can be observed in Figure 4. The dielectric loss factor is calculated through the following given equation.

Ɛ"= Ɛ' tan(δ)   (7)

Where tan (δ) is represented as tangent loss, (Ɛ') is the dielectric constant, and (Ɛ") is known as dielectric loss. From the above equation, dielectric constant and dielectric loss are directly related. The dielectric loss reflects the same trend as the dielectric constant. This dispersion is caused by interfacial polarization in the Maxwell-Wagner model and Koop's phenomenological theory. Hexa-ferrites exhibit polarization because of the hopping of electrons between Fe^{2+} and Fe^{3+}. High-resistance charge carriers encounter significant barriers at grain boundaries, leading to polarization. However, as the frequency of the applied electric field increases, the charge carriers fail to recognize the changing applied electric field, resulting in a polarization(Jadhav, Shirsath, Toksha, Shengule, & Jadhav, 2008). The measurement of the dielectric loss in polarization regarding changing fields is lagged.

The figure 4 gives the tan δ (dielectric loss factor) pattern to that of frequency. As predicted earlier, the peaks in this graph can be seen when the charge carrier's frequency becomes equal to that of the external electric field. This occurs due to the similarity of the ferrite conducting system and dielectric polarization. Based on this hypothesis, a potential clarification of the peaks in the above plot can be made (Ihsan Ali, Islam, Awan, & Ahmad, 2014).
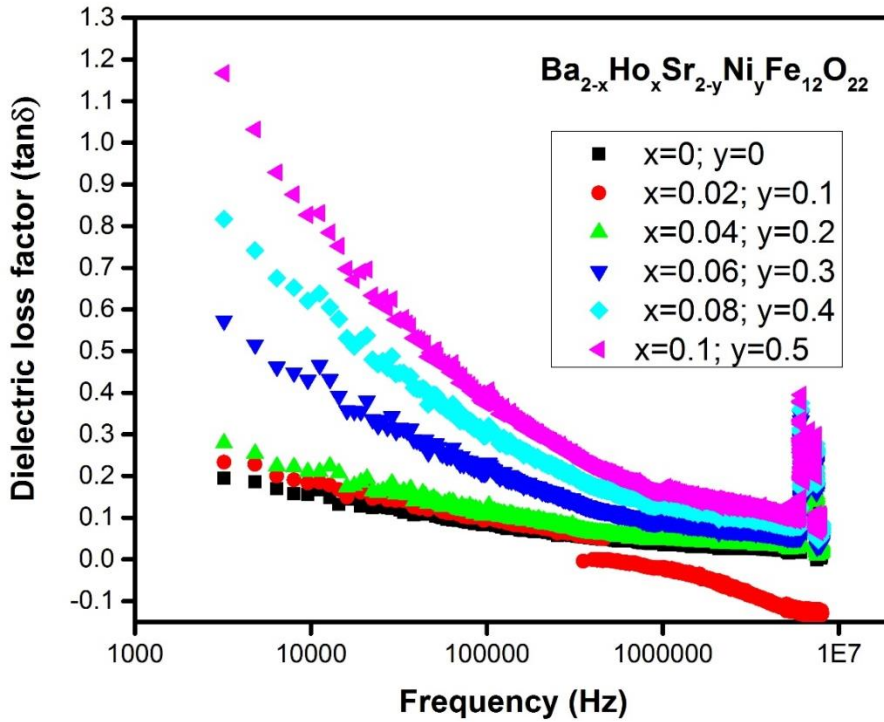
Figure 3: Frequency vs dielectric loss at room temperature

3.4. Impedance Spectroscopy

Standard impedance spectroscopy is used to examine the electrical properties of the samples, and it is carefully observed in terms of interfacial/electrode, grain, grain boundary, etc. The impedance technique records electrical responses at temperatures when a sinusoidal signal with a frequency of 1 KHz to 8 MHz is applied. The change in the impedance to the frequency is shown in Figure 5.The value of Z (Impedance) was found to be increasing with an increase in the Ho and Ni concentration in Ba-Sr hexagonal ferrites, which follows the dependence of AC conductivity on the composition. The increase in impedance gives rise to a decrease in AC conductivity. In comparison, the impedance decreases with an increase in frequency which causes an increase in the AC conductivity. The reduction in impedance and increase in AC conductivity with the increasing frequency gives the semiconducting behavior of the prepared samples(Khan et al., 2022).
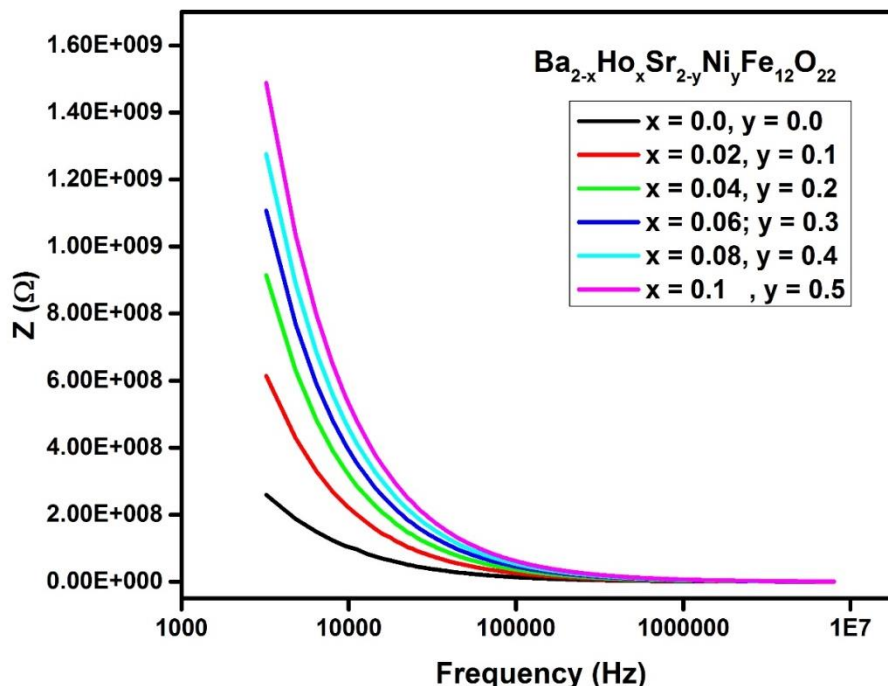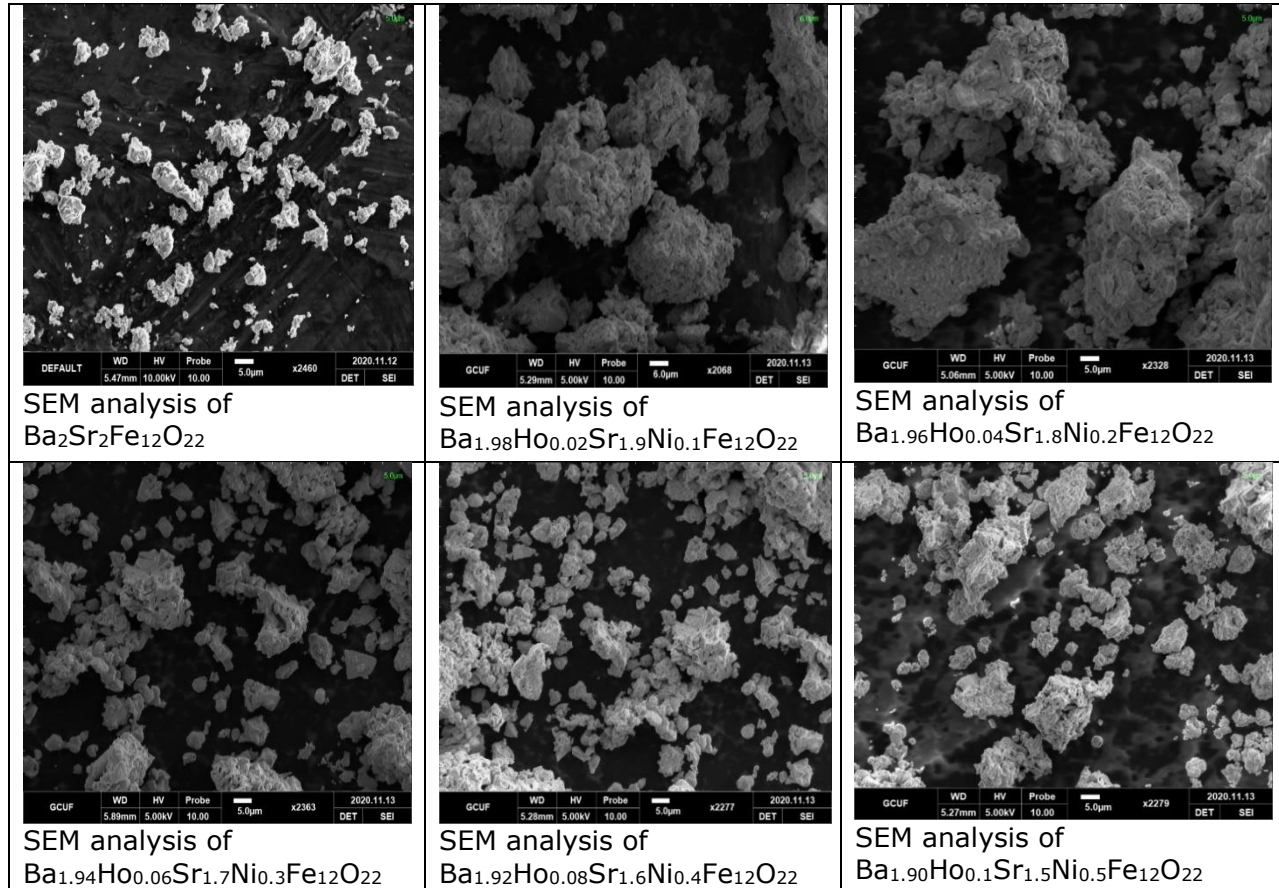

Figure 4: Frequency vs Impedance (Z) at room temperature

3.5. SEM Analysis

Scanning Electron Microscopy (SEM) is employed to disclose particle shape and morphology of the surface of synthesized y-type hexagonal ferrites $Ba_{2-x}Ho_xSr_{2-y}Ni_yFe_{12}O_{22}$. Figure 6shows the determined SEM images of the fabricated samples. The characteristic platelet-like structure of the grains, almost uniform particle dispersion, and high density are all visible in these micrographs. The grain size of the synthetic powders is assessed using the line intercept technique. The range of the determined grain size, which is between (0.83 µm–1.11 µm), is quite large. Higher sintering or calcination temperatures are the cause of the big grain size.

SEM analysis of $Ba_2Sr_2Fe_{12}O_{22}$

SEM analysis of $Ba_{1.98}Ho_{0.02}Sr_{1.9}Ni_{0.1}Fe_{12}O_{22}$

SEM analysis of $Ba_{1.96}Ho_{0.04}Sr_{1.8}Ni_{0.2}Fe_{12}O_{22}$

SEM analysis of $Ba_{1.94}Ho_{0.06}Sr_{1.7}Ni_{0.3}Fe_{12}O_{22}$

SEM analysis of $Ba_{1.92}Ho_{0.08}Sr_{1.6}Ni_{0.4}Fe_{12}O_{22}$

SEM analysis of $Ba_{1.90}Ho_{0.1}Sr_{1.5}Ni_{0.5}Fe_{12}O_{22}$

Figure 5: SEM Analysis of $Ba_{2-x}Ho_xSr_{2-y}Ni_yFe_{12}O_{22}$ Nano ferrites calcined at 950 °C for 6 h

The analysis of the morphology of the grains of Ho and Ni substituted Ba-Sr hexagonal ferrites sintered at 950 ℃ for 6 hours was carried out vis SEM in the above figures. The clustering of formed grains may be due to grown particles having large surface areas and may also be due to attractive forces between the magnetic particles(Chauhan et al., 2018). The grain size was also found to be increasing with the substitution of Ho and Ni in the prepared samples. The grain morphology was found to be enhanced by the substitution of Ho and Ni in the Ba-Sr hexagonal ferrites. The grain size of the prepared samples was also calculated, and the average grain size was found to be 2µm.
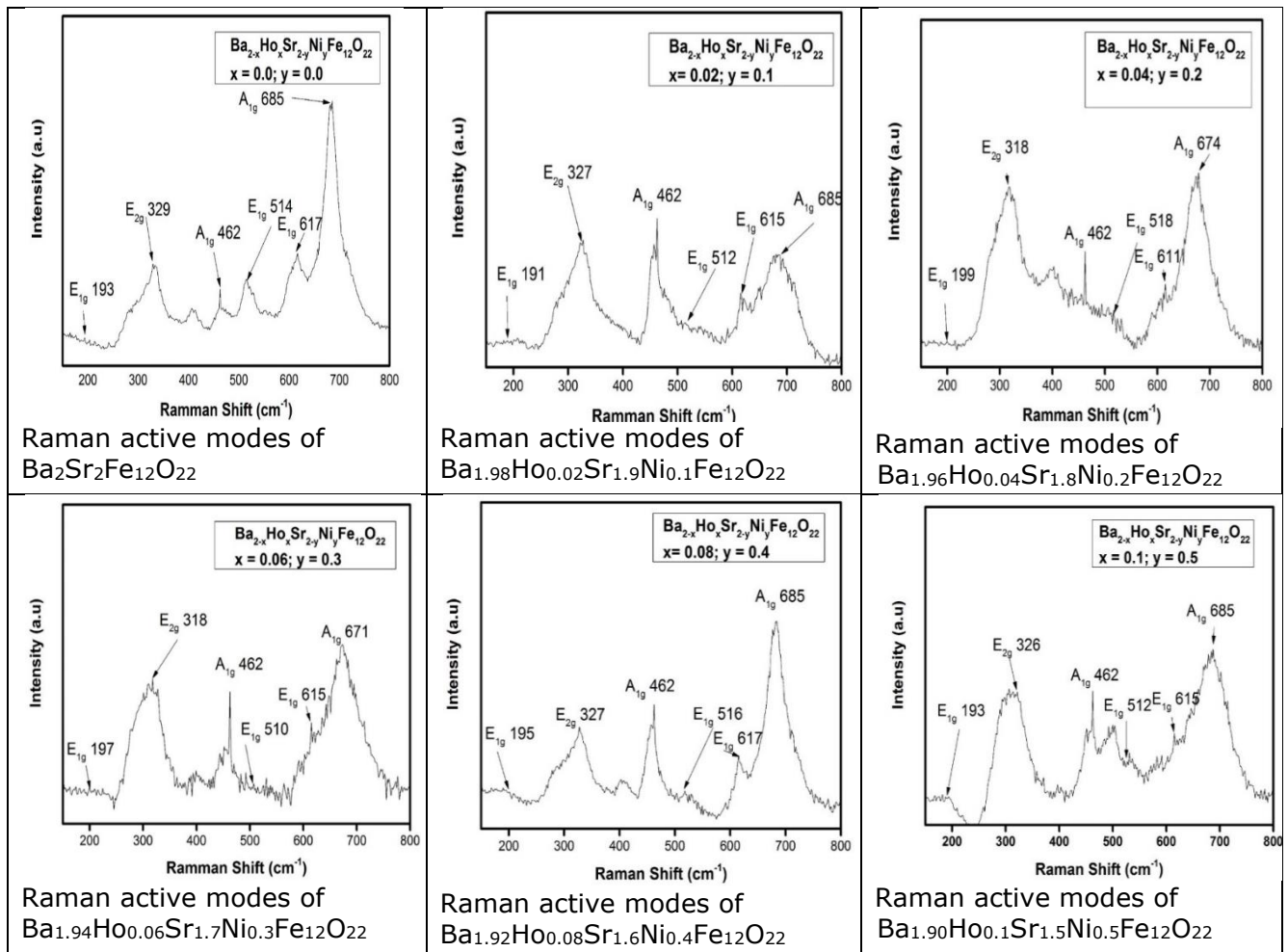
3.6. Raman Analysis

Raman spectroscopy is an innovative, non-destructive spectroscopy material identification technique used to provide information about structures comparable to one another and structural problems. Figure 7 shows the Raman spectra of synthesized$Ba_{2-x}Ho_xSr_{2-y}Ni_yFe_{12}O_{22}$ hexagonal ferrites (x = 0, 0.02, 0.04, 0.06, 0.08, 0.1 & y = 0, 0.1, 0.2, 0.3, 0.4, 0.5) nanomaterials ranged from 150 to-800 cm^{-1}. The Raman spectra of Hoand Ni substituted Ba-Sr hexagonal ferrites are displayed in Figure 7. Out of 42 Raman active modes (11A$_{1g}$, 14E$_{1g}$, 17E$_{2g}$), six active Raman modes are found, which corresponds to different vibrational modes (Table 2).

Table 2
Raman active modes of $B_{2-x}Ho_xSr_{2-y}Ni_yFe_{12}O_{22}$ (x = 0-0.1 and y = 0- 0.5) hexagonal ferrites

Concentration	E_{1g} (cm^{-1})	E_{2g} (cm^{-1})	A_{1g} (cm^{-1})	E_{1g} (cm^{-1})	E_{1g} (cm^{-1})	A_{1g} (cm^{-1})
x= 0, y=0	193	329	462	514	617	685
x= 0.02, y=0.1	191	327	462	512	615	685
x= 0.04, y=0.2	199	318	462	518	611	674
x= 0.06, y=0.3	197	318	462	510	615	671
x= 0.08, y=0.4	195	327	462	516	617	685
x= 0.1, y=0.5	193	326	462	512	615	685

E_{1g} mode is found to be in the range of 191-199 cm^{-1}, which is designated as a vibrational mode of the whole spinel block because of E_{1g} symmetry. E_{2g} mode is found to be in the range of 318-329 cm^{-1}, which is designated as the vibrational mode of the octahedral 2k site because of E_{2g} symmetry. A_{1g} mode is found to be 462 cm^{-1} due to the vibrational mode of octahedral 2k sites because of A_{1g} symmetry. E_{1g} mode is in the range of 510- 516 cm^{-1} due to the metal oxide bond vibration at the octahedral 2a and 2k sites because of E_{1g} symmetry. A_{1g} mode is in the range of 611- 617 cm^{-1} due to the stretching vibration of the Fe-O bond at the $4f_2$ octahedralsite because of A_{1g} symmetry. A_{1g} mode is in the range of 671- 685 cm^{-1}, due to the vibration mode of pyramidal 2b sites because of A_{1g} symmetry that makes a difference between spinel and hexagonal structure(Khalaf, Abd El-Lateef, Alnajjar, & Mohamed, 2020).

Raman active modes of $Ba_2Sr_2Fe_{12}O_{22}$

Raman active modes of $Ba_{1.98}Ho_{0.02}Sr_{1.9}Ni_{0.1}Fe_{12}O_{22}$

Raman active modes of $Ba_{1.96}Ho_{0.04}Sr_{1.8}Ni_{0.2}Fe_{12}O_{22}$

Raman active modes of $Ba_{1.94}Ho_{0.06}Sr_{1.7}Ni_{0.3}Fe_{12}O_{22}$

Raman active modes of $Ba_{1.92}Ho_{0.08}Sr_{1.6}Ni_{0.4}Fe_{12}O_{22}$

Raman active modes of $Ba_{1.90}Ho_{0.1}Sr_{1.5}Ni_{0.5}Fe_{12}O_{22}$

Figure 7: Raman Spectra of B $_{2-x}Ho_xSr_{2-y}Ni_yFe_{12}O_{22}$ hexagonal ferrites at room temperature

Conclusion

Y-type hexagonal ferrites with composition$B_{2-x}Ho_xSr_{2-y}Ni_yFe_{12}O_{22}$ aresynthesized viasol–gel method followed by an auto-combustion.XRD experiment confirmed the formation of pure phased Y-type hexagonal structure with no impurity traces. A significant

development was observed in the primary lattice parameter "c" axis. The crystalline size (5.67to 52.05 nm), lattice constant a(6.08 – 6.17 Å), and that of c (44.08 – 44.73 Å) displayed significant variation as a function of Ho-Ni concentration. SEM study revealed an average grain sizeto be 2μm. The dielectric constant and dissipation factor decreased due to the Fe^{2+} and Fe^{3+} ions exchange. Dispersion in the dielectric constant can be found due to the dipole's relaxation.Raman spectroscopy of Ho-Ni Nano ferritesrevealed six active modes, namely ($3E_{1g}$, $2A_{1g}$, and E_{2g}), corresponding to different vibrational modes of the prepared samples.

Reference

Ahmad, M., Ahmad, M., Ali, I., Ahmad, W., Mustafa, G., Akhtar, M. N., . . . Abbas, G. (2015). Temperature dependent structural and magnetic behavior of Y-type hexagonal ferrites synthesized by sol–gel autocombustion. *Journal of Alloys and Compounds, 651*, 749-755.

Ahmad, M., Ali, I., Grössinger, R., Kriegisch, M., Kubel, F., & Rana, M. (2013). Effects of divalent ions substitution on the microstructure, magnetic and electromagnetic parameters of Co2W hexagonal ferrites synthesized by sol–gel method. *Journal of Alloys and Compounds, 579*, 57-64.

Ali, I., Islam, M., Ashiq, M. N., Iqbal, M. A., Khan, H. M., & Murtaza, G. (2014). Role of grain boundaries in the conduction of Eu–Ni substituted Y-type hexaferrites. *Journal of Magnetism and Magnetic Materials, 362*, 115-121.

Ali, I., Islam, M., Karamat, N., Iftikhar, A., Shah, A., Athar, M., . . . Ashiq, M. N. (2015). Synthesis and magnetic properties of (Eu–Ni) substituted Y-type hexaferrite by surfactant assisted co-precipitation method. *Journal of Magnetism and Magnetic Materials, 385*, 386-393.

Aslibeiki, B. (2014). Nanostructural, magnetic and electrical properties of Ag doped Mn-ferrite nanoparticles. *Current Applied Physics, 14*(12), 1659-1664.

Batool, S. R., Malana, M. A., Alfryyan, N., Ashiq, M. N., Aftab, F., Aman, S., . . . Alomairy, S. (2022). Synthesis, characterization, dielectric and magnetic properties of substituted Y-type hexaferrites. *Journal of Materials Science: Materials in Electronics, 33*(20), 16183-16196.

Chauhan, C. C., Kagdi, A. R., Jotania, R. B., Upadhyay, A., Sandhu, C. S., Shirsath, S. E., & Meena, S. S. (2018). Structural, magnetic and dielectric properties of Co-Zr substituted M-type calcium hexagonal ferrite nanoparticles in the presence of α-Fe2O3 phase. *Ceramics International, 44*(15), 17812-17823.

Chen, X., Wang, Y., Liu, H., Jin, S., & Wu, G. (2022). Interconnected magnetic carbon@ NixCo1-xFe2O4 nanospheres with core–shell structure: An efficient and thin electromagnetic wave absorber. *Journal of Colloid and Interface Science, 606*, 526-536.

Din, M. F., Ahmad, I., Ahmad, M., Farid, M., Iqbal, M. A., Murtaza, G., . . . Khan, M. A. (2014). Influence of Cd substitution on structural, electrical and magnetic properties of M-type barium hexaferrites co-precipitated nanomaterials. *Journal of Alloys and Compounds, 584*, 646-651.

Elahi, A., Ahmad, M., Ali, I., & Rana, M. (2013). Preparation and properties of sol–gel synthesized Mg-substituted Ni2Y hexagonal ferrites. *Ceramics International, 39*(2), 983-990.

Houbi, A., Aldashevich, Z. A., Atassi, Y., Telmanovna, Z. B., Saule, M., & Kubanych, K. (2021). Microwave absorbing properties of ferrites and their composites: A review. *Journal of Magnetism and Magnetic Materials, 529*, 167839.

Irfan, M., Elahi, A., & Shakoor, A. (2016). Hysteresis and electric modulus analysis of Y3+ doped MnNi-Y-type hexagonal ferrite. *Ceramics–Silikáty, 60*(1), 34-40.

Jacobo, S., Domingo-Pascual, C., Rodriguez-Clemente, R., & Blesa, M. Publication: Journal of Materials Science Pub Date: 1997.

Jadhav, S. S., Shirsath, S. E., Toksha, B., Shengule, D., & Jadhav, K. (2008). Structural and dielectric properties of Ni-Zn ferrite nanoparticles prepared by co-precipitation method. *Journal of optoelectronics and advanced materials, 10*(10), 2644-2648.

Khalaf, M. M., Abd El-Lateef, H. M., Alnajjar, A. O., & Mohamed, I. M. (2020). A facile chemical synthesis of CuxNi (1− x) Fe2O4 nanoparticles as a nonprecious ferrite material for electrocatalytic oxidation of acetaldehyde. *Scientific Reports, 10*(1), 2761.

Khan, S. A., Ali, I., Hussain, A., Javed, H. M. A., Turchenko, V. A., Trukhanov, A. V., & Trukhanov, S. V. (2022). Synthesis and Characterization of Composites with Y-Hexaferrites for Electromagnetic Interference Shielding Applications. *Magnetochemistry, 8*(12), 186.

Kumazawa, H., Maeda, Y., & Sada, E. (1995). Further consideration of hydrothermal synthesis of barium ferrite fine particles. *Journal of materials science letters, 14*(1), 68-70.

Lan, D., Zhao, Z., Gao, Z., Kou, K., & Wu, H. (2021). Novel magnetic silicate composite for lightweight and efficient electromagnetic wave absorption. *Journal of Materials Science & Technology, 92*, 51-59.

Lassoued, A., & Li, J. (2020). Magnetic and photocatalytic properties of Ni–Co ferrites. *Solid State Sciences, 104*, 106199.

Liu, C., Liu, X., Feng, S., Rehman, K. M. U., Li, M., Zhang, C., . . . Meng, X. (2018). Effect of Y-La-Co substitution on microstructure and magnetic properties of M-type strontium hexagonal ferrites prepared by ceramic method. *Journal of Magnetism and Magnetic Materials, 445*, 1-5.

Majeed, A., Khan, M. A., ur Raheem, F., Ahmad, I., Akhtar, M. N., & Warsi, M. F. (2016). Morphological, Raman, electrical and dielectric properties of rare earth doped X-type hexagonal ferrites. *Physica B: Condensed Matter, 503*, 38-43.

Narang, S. B., & Pubby, K. (2021). Nickel spinel ferrites: a review. *Journal of Magnetism and Magnetic Materials, 519*, 167163.

Pant, R., Arora, M., Kaur, B., Kumar, V., & Kumar, A. (2010). Finite size effect on Gd3+ doped CoGdxFe2− xO4 (0.0≤ x≤ 0.5) particles. *Journal of Magnetism and Magnetic Materials, 322*(22), 3688-3691.

Pillai, V., Kumar, P., & Shah, D. (1992). Magnetic properties of barium ferrite synthesized using a microemulsion mediated process. *Journal of Magnetism and Magnetic Materials, 116*(3), L299-L304.

Rezlescu, N., Istrate, S., Rezlescu, E., & Luca, E. (1974). Cation distribution and Curie temperature in ferrites. *Journal of Physics and Chemistry of Solids, 35*(1), 43-46.

Wang, C.-h., Liu, Y., Luo, J.-r., Zheng, S.-K., Tu, J., Xu, H.-y., . . . Wang, P.-h. (2022). Deformation substructure development in AlXCoCrFeNi (X= 0, 0.3) high entropy alloy under different influencing factors. *Journal of Alloys and Compounds, 893*, 162196.

Wang, J., Ponton, C., & Harris, I. (2006). A study of Sm-substituted SrM magnets sintered using hydrothermally synthesised powders. *Journal of Magnetism and Magnetic Materials, 298*(2), 122-131.

Yang, B., & Wang, Z. (2017). Structure and magnetic properties of Mg0. 35Cu0. 2Zn0. 45Fe2O4 ferrite synthesized by co-precipitation method. *AIP Advances, 7*(5), 056114.

Zhong, W., & Ding, W. (1997). mad Zhmag, N.,". *Key Step in Synthesis of Ultrafme BaFel: O19 by Sol-Gel TechniqueS'al Magn. Mag. Mater, 168*, 196.